The Quantum Speed Limit of Optimal Controlled Phasegates for Trapped Neutral Atoms

Michael H. Goerz,[1,2,*] Tommaso Calarco,[3] and Christiane P. Koch[1,2,†]

[1] *Institut für Theoretische Physik, Freie Universität Berlin, Arnimallee 14, D-14195 Berlin, Germany*
[2] *Institut für Physik, Universität Kassel, Heinrich-Plett-Str. 40, D-34132 Kassel, Germany*
[3] *Institut für Quanteninformationsverarbeitung, Universität Ulm, D-89069 Ulm, Germany*

(Dated: January 18, 2013)

We study controlled phasegates for ultracold atoms in an optical potential. A shaped laser pulse drives transitions between the ground and electronically excited states where the atoms are subject to a long-range $1/R^3$ interaction. We fully account for this interaction and use optimal control theory to calculate the pulse shapes. This allows us to determine the minimum pulse duration, respectively, gate time T that is required to obtain high fidelity. We accurately analyze the speed limiting factors, and we find the gate time to be limited either by the interaction strength in the excited state or by the ground state vibrational motion in the trap. The latter needs to be resolved by the pulses in order to fully restore the motional state of the atoms at the end of the gate.

arXiv:1103.6050v1 [quant-ph] 30 Mar 2011

I. INTRODUCTION

The physical realization of a quantum computer requires the implementation of a set of universal gates [1]. The most difficult part is generally the two-qubit gate since it involves interaction between two otherwise isolated quantum systems. In proposals for quantum computing with ultracold neutral-atom collisions [2, 3], the two-qubit gate operation involves atomic motional degrees of freedom [4, 5], most often following adiabatic processes. This implies frequencies much lower than those characteristic of the trap, typically around a few tens of kHz. When long-range interactions, like dipole-dipole forces between Rydberg atoms [6–8], are employed, the relevant energy scales are larger and gate speed can in principle reach a few GHz.

Here, we study the limits to the two-qubit gate operation time for resonant excitation of two ultracold atoms into an electronically excited molecular state. This may be a low-lying state, like those used for photoassociating two atoms to form a molecule [9, 10], or high-lying Rydberg states [6–8]. In this scenario, the system dynamics becomes more complex, involving motion under the influence of the excited state potential. A high-fidelity gate can then no longer be designed "by hand". Fortunately, since any gate operation corresponds to a unitary transformation on the qubit basis, its implementation can be formulated as a coherent control problem [11, 12]. Solutions to the control problem can be found theoretically within the framework of optimal control [13–15]. Such an approach has been explored theoretically for molecular quantum computing with qubits encoded in vibrational states [11, 16]. Experimentally the control problem is solved using femtosecond laser pulse shaping combined with feedback loops [17]. Implementation of single-qubit gates with shaped picosecond pulses has recently been demonstrated for a qubit encoded in hyperfine levels of an atomic ion [18]. In this experiment, the fundamental limit to the gate operation time is set by the inverse of the hyperfine splitting since the hyperfine dynamics are required to realize arbitrary qubit rotations. The gate duration is in particular much shorter than the period of atomic motion in the trap [18].

Our goal is to implement a controlled phasegate,

$$\hat{\mathbf{O}} = \mathrm{diag}\left(e^{i\chi}, 1, 1, 1\right), \tag{1}$$

between two qubits carried by neutral atoms. Shaped short laser pulses are used to drive transitions into an electronic state where the two atoms are interacting. Obviously, the minimum gate operation time will depend on the interaction strength. A second timescale comes into play because the interaction couples electronic and nuclear dynamics, inducing vibrational excitations of the two atoms. The vibrational period of the trap might thus also affect the minimum gate operation time.

The limit to how fast a quantum gate can be performed is closely related to the minimum time it takes for a quantum system to evolve from an initial state to an orthogonal state, see for example [19] and references therein. This bound has been named the quantum speed limit; it is given in terms of the average energy and energy uncertainty of the quantum evolution [20]. Since evaluation of the bound requires knowledge of the full spectrum, one can typically evaluate it analytically only for simple model systems. Numerically, the bound can be determined using optimal control where the breakdown of convergence indicates that the quantum speed limit has been reached [21]. The following procedure allows us to determine the quantum speed limit for our desired two-qubit gate: We first set the gate operation time to a sufficiently large value to obtain a high fidelity implementation by optimal control. Then we reduce the gate time until the optimization algorithm cannot anymore find a high-fidelity solution. Analysis of the fairly complex system dynamics reveals which part of the overall system

*Electronic address: goerz@physik.uni-kassel.de
†Electronic address: christiane.koch@uni-kassel.de

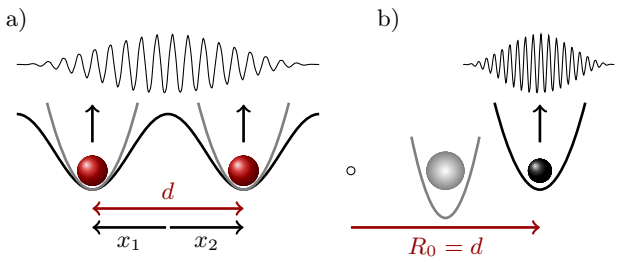

FIG. 1: (color online) Two calcium atoms in neighboring sites of an optical lattice (a), separated by distance d. The lattice potential can be taken in a harmonic approximation, allowing to separate the motion of both atoms into the center-of-mass motion and the interatomic motion (b). A phasegate is implemented by applying a shaped short laser pulse.

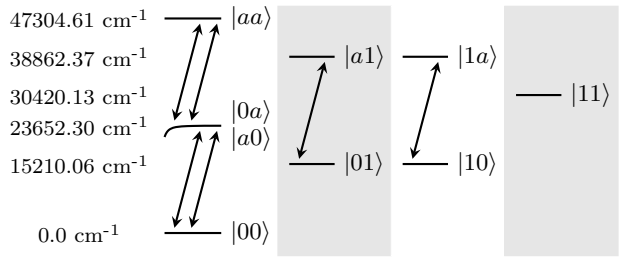

FIG. 2: Levels and laser-induced transitions for two qubits encoded in electronic states of two calcium atoms.

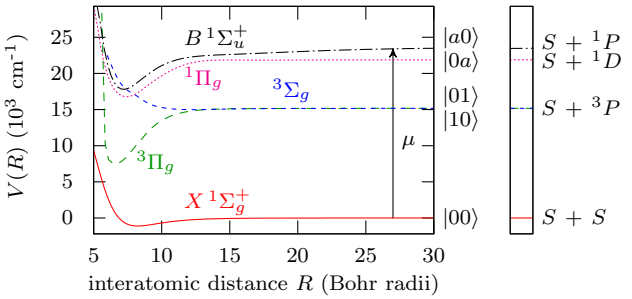

FIG. 3: (color online) Potential energy curves describing the interaction of two calcium atoms in the five lowest electronic states. The asymptotic values corresponding to $R = \infty$ are indicated on the right.

dynamics limits the gate operation time.

We consider neutral atoms trapped in optical tweezers or in neighboring sites of an optical lattice (Fig. 1). The sites to the right and left of the atom pair are assumed to be empty. We first consider alkaline-earth atoms which possess extremely long-lived excited states, cf. Ref. [22] and references therein. The qubits can therefore be encoded directly in the electronic states, that is, the atomic ground state $^1S_0$ together with the $^3P_1$ clock-transition state form a qubit. The laser is slightly detuned from the dipole allowed atomic transition between the $^1S_0$ ground state and the $^1P_0$ excited state, exciting the atom pair into the $B^1\Sigma_u^+$ molecular state. When both atoms are in the ground state, their interaction is of van-der-Waals type and practically zero at the trap distance. Due to different exchange interaction in the electronically excited state, the $B^1\Sigma_u^+$ state scales as $1/R^3$ at long range. This interaction may be employed to entangle the qubits provided the time that the atom pair resides in this state is much shorter than its lifetime of a few nanoseconds. The interaction strength is determined by the distance of the atoms. For realistic lattice parameters, $d \geq 200\,\mathrm{nm}$, the interaction is too weak to generate entanglement in a sufficiently short time. On the other hand, we would like to probe what are the factors that limit the achievable speed on a general level. To this aim, we first explore a regime that cannot be realized in experiments, but presents a clear separation of timescales that allows for a clearer interpretation of the dynamics. We start assuming a fictitious distance of $d = 5\,\mathrm{nm}$ and a correspondingly unrealistic atomic trap frequency of 400 MHz. This allows us to identify the limiting factors for fidelity and gate time. Formally, our Hamiltonian is equivalent to the one yielding a Rydberg phasegate for alkali atoms [6]. We therefore study in a second step the implementation of a phasegate based on very strong dipole-dipole interaction in the excited state for realistic lattice spacings. In particular, we seek to answer the question whether excitation of the vibrational motion can be avoided if the excited state interaction is strong enough to allow for very short gate pulses.

The paper is organized as follows. Section II introduces our model for the two atoms and summarizes how quantum gates can be implemented using optimal control theory. The numerical results are presented in Sec. III with Sec. III A devoted to generation of entanglement for two calcium atoms via interaction in the $B^1\Sigma_u^+$ state. A generic dipole-dipole interaction, $-C_3/R^3$, is considered in Sec. III B where we determine the gate operation time for varying C_3. We draw our conclusions in Sec. IV.

II. THEORETICAL APPROACH

A. Modeling Two Atoms in an Optical Lattice

We consider the following qubit encoding in a single calcium atom: The $^1S_0$ ground state corresponds to the qubit state $|0\rangle$ and is used to define the zero of energy. The $^3P_1$ first excited state, taken to be the qubit state $|1\rangle$, then occurs at $E_1 = 15210\,\mathrm{cm}^{-1}$. We consider the $^1P_1$ level as auxiliary state, $|a\rangle$, with energy $E_a = 23652\,\mathrm{cm}^{-1}$. For two atoms we then obtain nine electronic states $|00\rangle$, $|01\rangle$, $|0a\rangle$, $|10\rangle$, $|11\rangle$, $|1a\rangle$, $|a0\rangle$, $|a1\rangle$, with asymptotic energies $E_{ij} = E_i + E_j$ for the states $|ij\rangle$ $(i, j = 0, 1, a)$. This is depicted in Fig. 2. With the laser tuned close to the transition $|0\rangle \leftrightarrow |a\rangle$, no further electronic states will be resonantly populated. The potentials describing the interaction between the two atoms in the five lowest electronic states are shown in Fig. 3. The $X^1\Sigma_g^+$ ground state

potential corresponding to the two-qubit state $|00\rangle$ shows a $1/R^6$ behavior at long range such that the atoms are effectively non-interacting at any relevant distance, while the auxiliary $B^1\Sigma_u^+$ state corresponding to $|0a\rangle$ and $|a0\rangle$ goes as $1/R^3$. The remaining potentials corresponding to the two-qubit states $|aa\rangle$, $|a1\rangle$, $|1a\rangle$, $|11\rangle$, $|10\rangle$, and $|01\rangle$, are also essentially zero at the relevant distances. The potentials and transition dipole moment functions employed in the following calculations are gathered from Refs. [23, 24]. For a Rydberg phasegate with alkali atoms, the qubit encoding is the standard one in hyperfine levels of the electronic ground state; and the auxiliary level corresponds to the Rydberg state (we omit in this description any intermediate level that might be needed for near-resonant two-photon excitation of the Rydberg state). In this case, the ground state potential is simply set to zero, while the auxiliary state is modeled by a generic C_3/R^3 potential.

The parameters of the optical lattice are chosen such that the motion of the atoms is restricted to one spatial dimension ($\omega_\perp \gg \omega_0$). Approximating the resulting trapping potential for the two atoms by two displaced harmonic oscillators, we can separate the center of mass coordinate which is subsequently integrated out, and the relative coordinate, i.e. the interatomic distance R.

The Hamiltonian of our model, taking into account the nine two-qubit states, the motion in the trap, and the interaction between the atoms, is given by

$$\begin{aligned}\hat{\mathbf{H}} &= \hat{\mathbf{H}}_{1q}\otimes\mathbb{1}_{1q}\otimes\mathbb{1}_R + \mathbb{1}_{1q}\otimes\hat{\mathbf{H}}_{1q}\otimes\mathbb{1}_R + \hat{\mathbf{H}}_{\rm int}\\ &= \sum_{i,k}|ik\rangle\langle ik|\left[\hat{\mathbf{T}}+\hat{\mathbf{V}}_{\rm trap}(R)+\hat{\mathbf{V}}^{ik}_{BO}(R)+E_{ik}\right]\\ &\quad +\epsilon(t)\sum_{i\neq j,k}\left[\,|ik\rangle\langle jk|+|ki\rangle\langle kj|\,\right]\otimes\hat{\boldsymbol{\mu}}_{ij}(R). \qquad (2)\end{aligned}$$

Here, $\hat{\mathbf{H}}_{1q}$ denotes the Hamiltonian for a single three-level atom, $\mathbb{1}_{1q}$ is the identity in $SU(3)$, and $\mathbb{1}_R$ represents the identity for the motional degree of freedom. The interaction Hamiltonian $\hat{\mathbf{H}}_{\rm int}$ contains the Born-Oppenheimer potentials $\hat{\mathbf{V}}_{BO}$, and the laser pulse $\epsilon(t)$ couples to the transition dipoles $\hat{\boldsymbol{\mu}}_{ij}$. The indexes i,j,k each run over $0,1,a$. The Hamiltonian, Eq. (2), is represented on a Fourier grid with variable step size [25–27].

A two-qubit gate is successfully implemented if the four basis states $|00\rangle$, $|01\rangle$, $|10\rangle$, $|11\rangle$ transform according to the desired unitary transformation $\hat{\mathbf{O}}$. Initially, the wavefunction for the motional degree of freedom is given in terms of two atoms in the ground state of the displaced harmonic oscillators, $\varphi_0(R) = \langle R|\varphi_0\rangle$. Hence we consider four initial states given by $|ij(R)\rangle = |ij\rangle\otimes|\varphi_0\rangle$, $i,j=0,1$. The dynamics induced by a laser pulse will populate other states in the full $3\times3\times N_R$-dimensional Hilbert space (with N_R the number of grid points to represent the motional degree of freedom); that is, it will induce internuclear motion leading out of the logical subspace. In order to calculate the gate operation in the logical subspace at the end of the pulse, the final states are reduced to the logical basis by tracing out the motional degree of freedom after projection onto $|\varphi_0\rangle$.

B. Optimal Control Theory for a Two-Qubit Gate

In order to implement the target operation defined in Eq. (1), a suitable pulse $\epsilon(t)$ must be found that drives the system evolution such that $\hat{\mathbf{U}}(T,0;\epsilon) = \hat{\mathbf{O}}$. Optimal control treats the fidelity F, $F\in[0,1]$, which measures how close the evolved two-qubit basis states $\hat{\mathbf{U}}(T,0;\epsilon)\,|ij(R)\rangle$ come to the desired target states $\hat{\mathbf{O}}\,|ij(R)\rangle$, as a functional of the control field ϵ. Allowing for additional constraints such as minimization of the integrated pulse energy leads to the total functional J,

$$J = -F + \int_0^T g(\epsilon)\,{\rm d}t\,, \qquad (3)$$

which is to be minimized. Variation of the functional J with respect to the evolving two-qubit basis states and the control field yields a set of coupled optimization equations that need to be solved iteratively [12–15]. We use the linear Krotov algorithm as outlined in Ref. [12] to perform the optimization. Starting with an arbitrary guess pulse $\epsilon^{(k)}(t)$, $k=0$, the algorithm sequentially updates the pulse at every point in time to yield an optimized pulse $\epsilon^{(k+1)}(t)$ that is *guaranteed* to improve the target functional J in each step of the iteration k. We take the running cost $g(\epsilon)$ in Eq. (3) to be the change in integrated pulse energy,

$$g(\epsilon) = \frac{\alpha}{S(t)}\left[\epsilon^{(k+1)}(t)-\epsilon^{(k)}(t)\right]^2\,, \qquad (4)$$

rather than the integrated pulse energy itself. This guarantees that, as we approach the optimum, $g(\epsilon)$ goes to zero such that the minimum of J becomes equal to the maximum of F [12]. In Eq. (4), α denotes an arbitrary positive scaling parameter, and the shape function $S(t)$,

$$S(t) = \sin^2(\pi t/T)\,, \qquad (5)$$

ensures that the pulse is switched on and off smoothly.

A possible starting point to define the fidelity is given by the complex-valued inner matrix product [12],

$$\tau = \sum_{i,j=0,1}\left\langle ij(R)\left|\hat{\mathbf{O}}^\dagger\hat{\mathbf{U}}\right|ij(R)\right\rangle\,. \qquad (6)$$

Out of the several choices for obtaining a real-valued functional, we employ

$$F = \frac{1}{N}\mathfrak{Re}\left[\tau\right]\,, \qquad (7)$$

which is sensitive to a global phase [12]. The Hilbert space of the optimization problem can then be reduced to the $8N_R$-dimensional subspace since the $|11\rangle$ level has no coupling to any other level, see Fig. 2. The evolution

of the $|11(R)\rangle$ state cannot be controlled by the laser pulse but it is known to be

$$\hat{\mathbf{U}}(T,0;\epsilon)\,|11(R)\rangle = e^{i\phi_T}\,|11(R)\rangle\,; \quad \phi_T = E_{11}T/\hbar\,.$$

Including the information about the phase ϕ_T explicitly as a global phase for all target states $\hat{\mathbf{O}}\,|ij(R)\rangle$, the evolution of $|11(R)\rangle$ can be omitted from the system dynamics. Since entanglement is generated only by the dynamics of the states in the left-most column of Fig. 2, and the remaining levels remain uncoupled from the vibrational dynamics, the system dynamics can be further separated into those of the four molecular states in the left-most column of Fig. 2 and those of a two-level system representing the states in the middle columns of Fig. 2. Care must then be taken to extract the true two-qubit phase from the evolution of the $|00(R)\rangle$ state which contains two-qubit and single-qubit contributions. This is described in Appendix A. The numerical results presented below are obtained both within the $8N_R$-dimensional model and the $4N_R$-dimensional model plus two-level system, and the optimal pulses have been cross-checked.

For the fidelity defined in Eq. (7) and the running cost given in Eq. (4), the optimization equations read [12]

$$\Delta\epsilon(t) \;=\; \epsilon^{(k+1)}(t) - \epsilon^{(k)}(t) = \frac{S(t)}{2\alpha}\mathfrak{Im}\left[\sum_{i,j=0,1}\left\langle \Psi_{ij}^{bw}(R;t)\left|\hat{\boldsymbol{\mu}}_{ij}(R)\right|\Psi_{ij}^{fw}(R;t)\right\rangle\right], \tag{8}$$

$$\left\langle \Psi_{ij}^{bw}(R;t)\right| \;=\; \langle ij(R)|\,\hat{\mathbf{O}}^{\dagger}\hat{\mathbf{U}}^{\dagger}(t,T;\epsilon^{(k)})\,, \tag{9}$$

$$\left|\Psi_{ij}^{fw}(R;t)\right\rangle \;=\; \hat{\mathbf{U}}(t,0;\epsilon^{(k+1)})\,|ij(R)\rangle\,. \tag{10}$$

Here, $\left\langle \Psi_{ij}^{bw}(R;t)\right|$ denotes the backward propagated target state $\hat{\mathbf{O}}\,|ij(R)\rangle$ at time t. The backward propagation is carried out using the old field, $\epsilon^{(k)}(t)$. $\left|\Psi_{ij}^{fw}(R;t)\right\rangle$ represents the forward propagated initial state $|ij(R)\rangle$ at time t. The new field, $\epsilon^{(k+1)}(t)$, is employed in the forward propagation. $\left\langle \Psi_{ij}^{bw}(R;t)\right|$ and $\left|\Psi_{ij}^{fw}(R;t)\right\rangle$ are obtained by solving the time-dependent Schrödinger equation numerically with the Chebychev propagator [28]. The time is discretized in n_t steps of width Δt, between 0 and T. Since no rotating wave approximation is employed, Δt has to be fairly small (0.025 fs to 0.05 fs).

For the desired gate implementation, there are two aspects to the optimization problem: On one hand, the two-qubit phase χ has to be realized. This is possible due to the interaction between the two qubits in the electronically excited auxiliary state. On the other hand, control over the motional degree of freedom has to be exerted. That is, at the end of the gate operation, the motional states $|ij(R)\rangle = |ij\rangle \otimes |\varphi_0\rangle$ have to be fully restored, except for the phases ϕ_{ij}. Final wavefunctions containing contributions from eigenstates other than $|ij\rangle \otimes |\varphi_0\rangle$ imply leakage from the quantum register. These two aspects of the optimization result can be quantified independently, and allow for a more thorough analysis of the solutions to the control problem than just the fidelity.

The success of control over the motional degree of freedom for the ground state is measured by projecting the final state, $\hat{\mathbf{U}}(T,0;\epsilon^{opt})\,|00(R)\rangle$, onto the desired state,

$$F_{00} = \left|\left\langle 00(R)\left|\hat{\mathbf{U}}(T,0;\epsilon^{opt})\right|00(R)\right\rangle\right|^2. \tag{11}$$

The phase acquired by each of the propagated basis states is given by

$$\phi_{ij} = \arg\left(\left\langle ij(R)\left|\hat{\mathbf{U}}(T,0;\epsilon^{opt})\right|ij(R)\right\rangle\right). \tag{12}$$

The phases ϕ_{ij} contain both single-qubit and two-qubit contributions. This is due to the weak molecular interaction which corresponds to small detunings of the laser from the atomic transition line. The pulse therefore drives single-qubit purely atomic local transitions in addition to true two-qubit nonlocal transitions into the molecular state. The Cartan decomposition of a two-qubit unitary into local and non-local contributions provides a tool to extract the desired non-local phase χ from the ϕ_{ij}. It states that any two-qubit gate can be decomposed as $\hat{\mathbf{U}} = \hat{\mathbf{k}}_1\hat{\mathbf{A}}\hat{\mathbf{k}}_2$, where $\hat{\mathbf{k}}_1$ and $\hat{\mathbf{k}}_2$ are local operations acting on the single qubits, and $\hat{\mathbf{A}}$ is a non-local operator. The non-local contribution is characterized by local invariants [29]. For the phasegate considered here, the local invariants are calculated according to Ref. [29] to be

$$G_1\left(\hat{\mathbf{U}}\right) \;=\; \cos^2\left[\frac{1}{2}(\phi_{00}-\phi_{01}-\phi_{10}+\phi_{11})\right],$$

$$G_2\left(\hat{\mathbf{U}}\right) \;=\; 2+\cos\left[\phi_{00}-\phi_{01}-\phi_{10}+\phi_{11}\right].$$

On the other hand, for the desired target gate $\hat{\mathbf{O}}$ defined in Eq. (1), the local invariants are given by

$$G_1\left(\hat{\mathbf{O}}\right) = \cos^2\left[\frac{\chi}{2}\right], \quad G_2\left(\hat{\mathbf{O}}\right) = 2+\cos\left[\chi\right].$$

We can thus identify the non-local phase,

$$\chi = \phi_{00}-\phi_{01}-\phi_{10}+\phi_{11}\,. \tag{13}$$

The non-local character of the implemented gate $\hat{\mathbf{U}}$ can also be measured in terms of the entangling power or concurrence [30]. For the controlled phasegate it is obtained from the non-local phase χ,

$$C = \left|\sin\frac{\chi}{2}\right| . \tag{14}$$

In the presentation of our numerical results below we will use the motional purity F_{00} and the non-local phase χ in addition to the fidelity F to analyze the performance of the optimal pulses.

III. RESULTS

In order to obtain a clear physical picture of the limiting factors that influence the speed of the two-qubit gate operation, we start by exploring a regime in which the atom-atom interaction would be so strong to yield a time scale shorter than any other in the problem. This regime is experimentally unfeasible with optical potential both in terms of length scales and of confinement strengths, and in this sense the calculation represents little more than a toy model. Nevertheless, we simulate the dynamics taking into account in detail the physical features of a real atomic species *as if* the geometry considered were realizable in the laboratory via some trapping force. This allows us to gain a thorough understanding of the relevant energy and time scales, which we subsequently apply to a more realistic case of Rydberg-excited atoms interacting at longer distances, compatible with realistic optical potentials.

A. Optimization for Two Calcium Atoms at Short Distance

We consider two calcium atoms in an optical lattice at a distance of $d = 5\,\mathrm{nm}$ that will be excited into a low-lying excited state. While such a distance is not feasible with the trapping techniques currently available in experiments, larger distances do not provide a sufficient interaction strength in the excited state to reach any significant fidelity in a reasonable amount of time. Nevertheless, this unrealistic assumption allows us to determine the physical mechanisms that limit the gate operation time.

At close distance, the ground state wave functions of the two atoms in a harmonic trap can have a significant overlap,

$$\langle\Psi_+|\Psi_-\rangle \approx e^{-\frac{m\omega d^2}{2\hbar}} .$$

In order to be able to treat qubits carried by the two atoms as independent, we compensate for the small value of d with an artificially large trap frequency. A choice of $\omega = 400\,\mathrm{MHz}$ ensures that the overlap of the wave functions is smaller than 10^{-4}. The grid parameters need to be chosen such that a reasonable number of trap eigenstates (about 50 in our case) is correctly represented. This is accomplished by taking $R_{\min}$ to be $5.0\,a_0$, $R_{\max} = 300.0\,a_0$, the number of grid points $N_R = 512$, with mapping parameters $\beta = 0.5$, $E_{\max} = 1\times10^{-8}$, cf. Ref. [25].

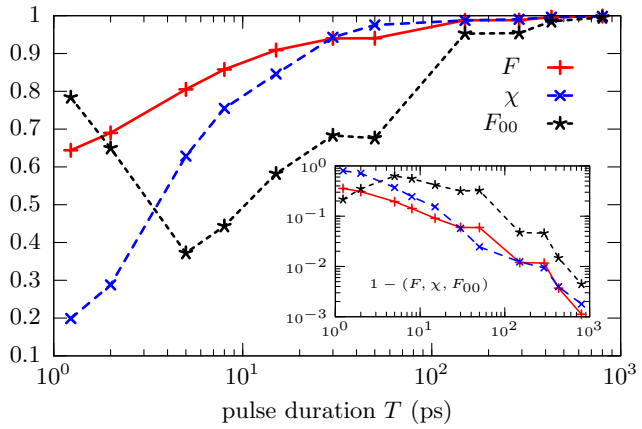

FIG. 4: (color online) Fidelity F, non-local phase χ (in units of π) and vibrational fidelity, i.e., projection onto the vibrational target state, F_{00}, for different gate times T. The inset shows the infidelity $1-F$ and the respective quantities $1-\chi$ and $1-F_{00}$.The interatomic distance is $d = 5\,\mathrm{nm}$.

The minimum gate operation time to achieve a high-fidelity implementation can be due to (i) the strength of the exchange interaction in the excited state, or (ii) the vibrational motion in the trap. We investigate both hypotheses. The time scale associated with the interaction strength is estimated from the maximum phase that can accumulate in the interacting state during time T. For a non-local phase of one radian, we find

$$T_{int}^{rad}(d) = \frac{1}{E_{0a} - V_{0a}(d)} , \tag{15}$$

where E_{0a} denotes the energy of two infinitely separated, i.e. non-interacting atoms in the $|0a\rangle$ or $|a0\rangle$ state, and $V_{0a}(d)$ the interaction potential at distance d. For $d = 5\,\mathrm{nm}$, this yields $T_{int}^{rad} \approx 1.23\,\mathrm{ps}$ for a non-local phase of one radian, and $T_{int}^{\pi} \approx 4.4\,\mathrm{ps}$ for a non-local phase of π. The time scale associated with the vibrational motion in the trap is estimated by considering the mean energy difference of the trap ground state energy to its neighboring levels, i.e. the last bound state and the first excited trap state. For the chosen trap frequency, we obtain $T_v \approx 800\,\mathrm{ps}$.

The optimization results for gate operation times varied between the two limits T_{int}^{rad} and T_v are shown in Figure 4. We compare fidelity F, Eq. (7), non-local phase χ, Eq. (13), and vibrational fidelity F_{00}, Eq. (11). The optimizations are converged to within $\Delta F < 1\times10^{-4}$ except for $T = 30$ ps and 50 ps which are converged to within $\Delta F < 2\times10^{-4}$. For durations below 150 ps, with errors remaining larger than 10^{-2} no satisfactory fidelity

is obtained. As the gate operation time approaches T_v, optimization is successful in the sense that fidelities arbitrarily close to one can be reached. The results shown in Fig. 4 can be understood as follows: The two-qubit phase χ increases with the pulse duration T, and at $T = 5\,\mathrm{ps}$, the time that was roughly estimated to reach a non-local phase of π, about half that phase is actually obtained. This is not surprising since the wavepacket is not in the excited state for the complete gate duration T due to the switch-on and switch-off phases of the pulse and its general shape. The non-local phase reaches the desired value of π at about 50 ps. We thus find that a prolonged action of the exchange interaction leads indeed to a non-local gate. However, for short gate durations, no control over the motional degree of freedom can be exerted. For $T = 5\,\mathrm{ps}$, the vibrational fidelity drops below 50%, and it increases rather slowly for larger T. This is due to the wave packet spending enough time in the excited state to be accelerated by the $1/R^3$ potential. When the laser pulse returns the wavepacket to the electronic ground state, it has acquired significant vibrational energy. Since the pulse is too short to resolve the vibrational motion in the trap, optimization cannot identify the desired trap state and thus it cannot counteract the excitation. Population of excited trap states after the gate can be avoided only once the pulse is long enough to resolve different trap states. As the gate duration becomes comparable to T_v, fidelities close to one are obtained.

An analysis of the dynamics induced by the optimized pulses is instructive for short gate durations despite the low fidelity. Figures 5 and 6 display the optimized pulse, its spectrum, and the dynamics for $T = 5\,\mathrm{ps}$. The guess pulse that is used to start the iterative optimization has a Gaussian envelope with a peak intensity of about $4.9 \times 10^7\,\mathrm{V/m}$. The intensity was chosen to drive one complete Rabi cycle for a single qubit in the $|0\rangle$ state (2π-pulse). The pulse fluence is increased by a factor of about 7 during the course of iterations. Optimization results in a pulse shape that clearly shows more features than a Gaussian, cf. top panel of Fig. 5. The first peak of the pulse, centered around $\approx 100\,\mathrm{fs}$, drives significant population transfer to the auxiliary state. The last peak of the pulse, centered around $\approx 1\,\mathrm{ps}$, restores all population to the electronic ground state. The dynamics yielding the non-local phase occur at intermediate times. Since there is no interaction between the two atoms in the $|01\rangle$ and $|a1\rangle$ states, the population dynamics of the $|01\rangle$ state (red dot-dashed line in Fig. 5) are equivalent to those of a single atom. Comparison of the population dynamics of the $|00\rangle$ state and the $|01\rangle$ state (black solid and red dot-dashed lines in the top panel of Fig. 5) therefore yields the difference between single-qubit and two-qubit dynamics. For the short gate operation time shown in Fig. 5, the two curves are fairly similar. This is in agreement with the non-local phase of only $0.63\,\pi$ that is achieved. The spectrum of the optimized pulse, cf. bottom panel of Fig. 5, is tightly centered around the $|0\rangle \rightarrow |a\rangle$ transition frequency of $23652.30\,\mathrm{cm}^{-1}$. It is

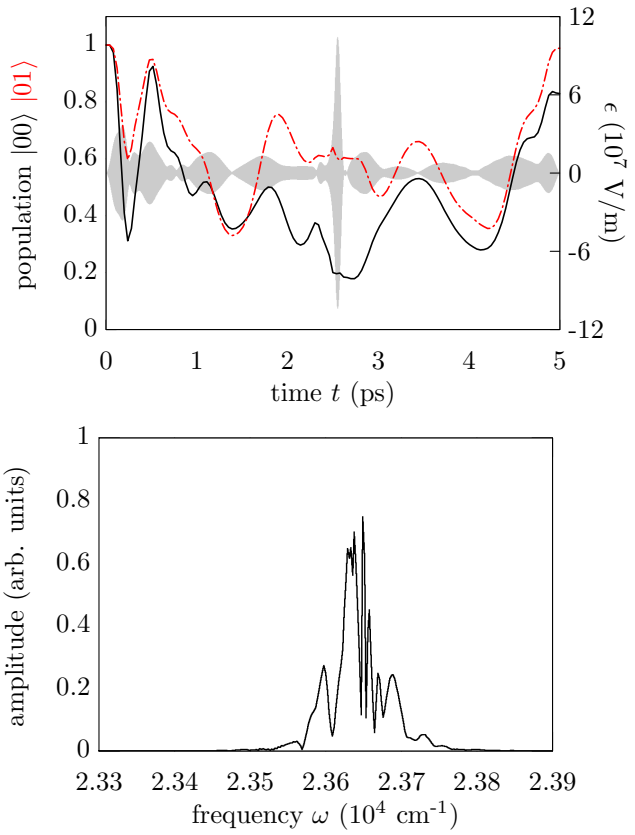

FIG. 5: (color online) Optimized pulse (gray) and population dynamics ($|00\rangle$ state: solid black line, $|01\rangle$ state: dot-dashed red line, top) and pulse spectrum (bottom) for $T = 5\,\mathrm{ps}$ ($F = 0.805$).

sufficiently narrow to guarantee that no undesired transitions, for example into the ${}^1\Pi_g(S+D)$ state, are induced.

The dynamics of the two-qubit system and of a single qubit can be analyzed by projecting the time-evolved two-qubit basis state onto the initial two-qubit and single-qubit states,

$$\tau_{ij}(t) = \left\langle ij(R) \left| \hat{\mathbf{U}}(t,0;\epsilon^{opt}) \right| ij(R) \right\rangle , \quad (16)$$

$$\tau_{j}(t) = \left\langle j \left| \hat{\mathbf{U}}(t,0;\epsilon^{opt}) \right| j \right\rangle . \quad (17)$$

The phase dynamics $\tau_{ij}(t)$ and $\tau_j(t)$ obtained with the optimized pulse of Fig. 5 are shown in Fig. 6 with the top (bottom) corresponding to the two-qubit (single-qubit) dynamics. The phase of the initial state is indicated by a filled black circle, the phase of the final state by a black square, and the phase of the optimization target by a blank circle. The phase dynamics of the $|01\rangle$ state (upper right panel of Fig. 6, no connecting lines are shown) consist of a mixture of the natural time evolution and the dynamics induced by the pulse. The $|1\rangle$ state (lower right panel of Fig. 6) displays *only* the natural time evolution. Since it is not coupled to any other state by the pulse, the population remains one, i.e., on the unit circle, at all

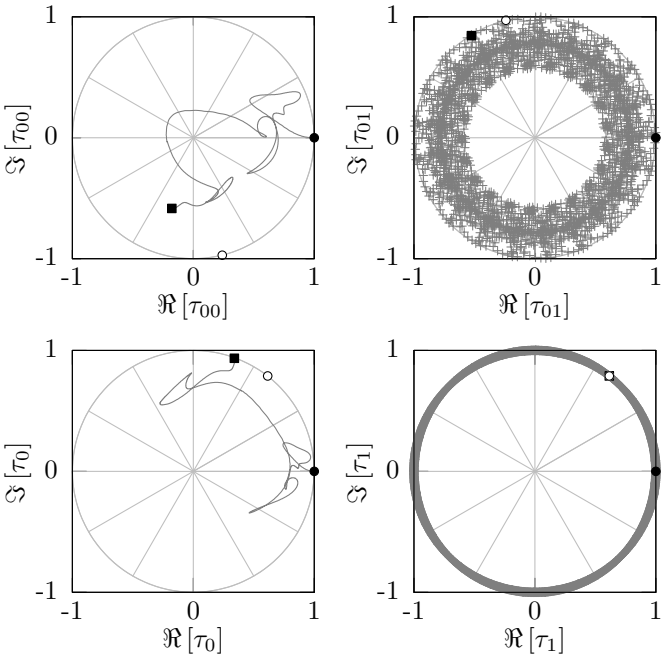

FIG. 6: Phase dynamics induced by the optimized pulse ($T = 5$ ps) in the complex plane for the two-qubit states (top) and the single-qubit states (bottom). The initial state is represented by a black circle, the final state by a black square, and the target state by a blank circle.

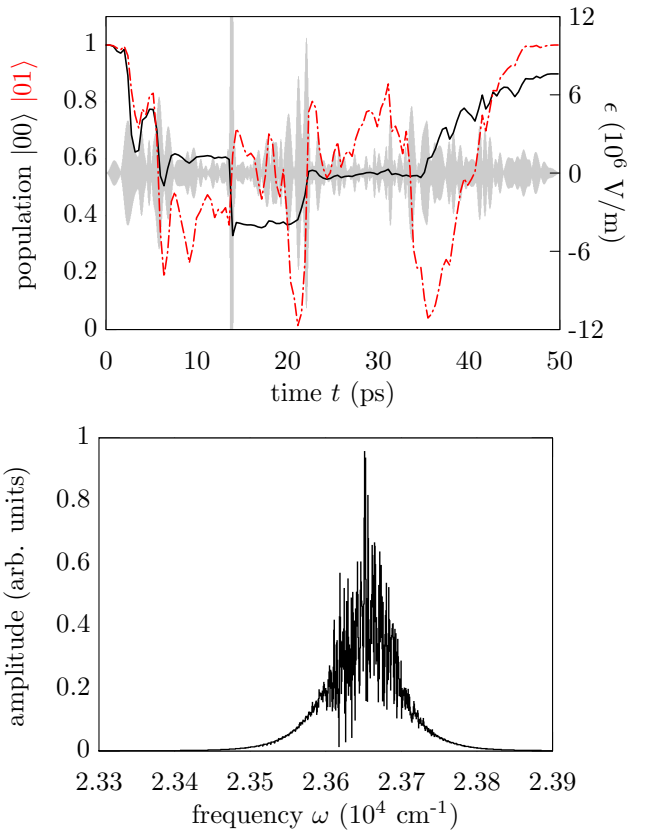

FIG. 7: (color online) Pulse dynamics (top) and spectrum (bottom) for the optimized pulse with $T = 50$ ps after 255 iterations($F = 0.988$), analogously to Fig. 5

times. The fact that the $|00\rangle$ state does not return to the unit circle at the final time T indicates leakage out of the quantum register. The overall fidelity amounts to only 0.805, cf. Figure 4, with the target phase for both the $|00\rangle$ state and $|01\rangle$ state missed by almost equal amounts, cf. black squares and empty circles in the upper panel of Fig. 6. This reflects that the optimization is balanced with respect to all targets, i.e. the terms in the sum of the target functional, Eqs. (6)-(7), all enter with the same weight. A comparison of the $|00\rangle$ and $|0\rangle$ phase dynamics (upper and lower left panels of Fig. 6) illustrates how a true non-local phase is achieved, even though the optimization is only partially successful: Without interaction the phase on the $|00\rangle$ state would evolve according to $\phi_{00} = 2\phi_0$. The extent to which this is not the case demonstrates how the interaction leads to the non-local phase.

The optimized pulses, their spectra, and the corresponding population dynamics for intermediate and long gate durations are shown in Figs. 7 ($T = 50$ ps) and 8 ($T = 800$ ps). The guess pulses were again chosen to be Gaussian 2π-pulses. During the course of the iterations, the pulse fluence was increased by a factor of 28 for $T = 50$ ps and by a factor of 44 for $T = 800$ ps. The overall structure of the optimized pulse for $T = 50$ ps is similar to that obtained for $T = 5$ ps: Two peaks at the beginning and the end induce population transfer to and from the auxiliary state while the intermediate part of the pulse drives Rabi oscillations in the course of which the non-local phase is achieved. The first peak of the pulse triggering population transfer to the auxiliary state remains clearly visible as the gate operation time T is further increased, cf. Fig. 8. Overall, however, the optimal pulse shows less discernible features for $T = 800$ ps than for the shorter gate durations where a sequence of subpulses was found. This is reflected in the population dynamics: While for $T = 50$ ps, each subpulse drives a partial transfer, resulting in step-wise population dynamics, an almost adiabatic behavior is observed for $T = 800$ ps. Comparing the population dynamics for a single qubit and the two-qubit system for $T = 50$ ps (black solid and red dot-dashed lines in the upper panel of Fig. 7), more differences are obtained than for $T = 5$ ps, cf. Fig. 5, but overall the single qubit and two-qubit dynamics are still fairly similar. This changes dramatically for $T = 800$ ps (black solid and red dot-dashed lines in the upper panel of Fig. 8), where the populations dynamics for $|00\rangle$ and $|01\rangle$ are clearly distinct, reflecting that the desired non-local phase is fully achieved ($\chi = 0.998\pi$ for $T = 800$ ps as compared to $\chi = 0.975\pi$ for $T = 50$ ps). The spectrum of the optimal pulse for $T = 50$ ps is fairly similar to that obtained for $T = 5$ ps, cf. the lower panels of Figs. 5 and 7: It basically consists of a single narrow peak centered around the $|0\rangle \rightarrow |a\rangle$ transition frequency. The spectrum

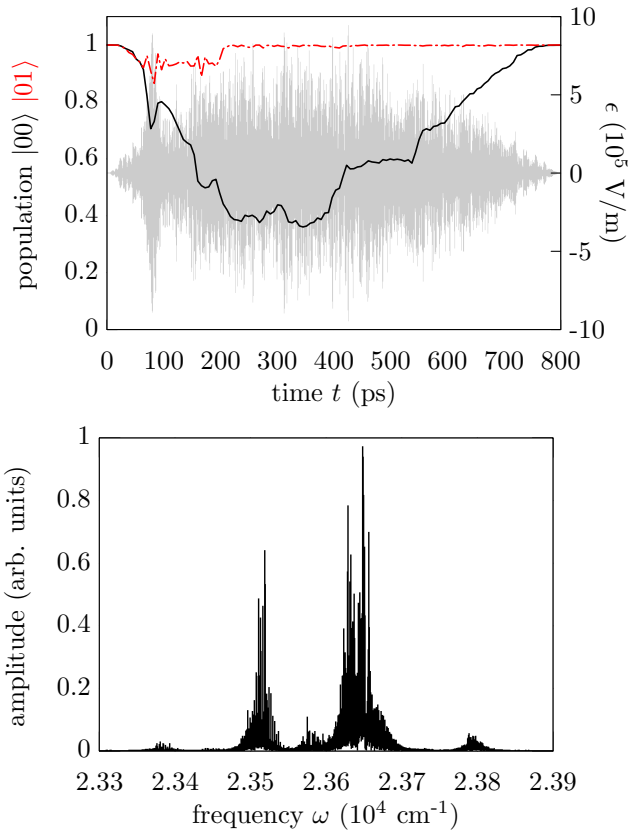

FIG. 8: (color online) Pulse dynamics (top) and spectrum (bottom) for the optimized pulse with $T = 800\,\text{ps}$ after 104 iterations ($F = 0.999$), analogously to Fig. 5

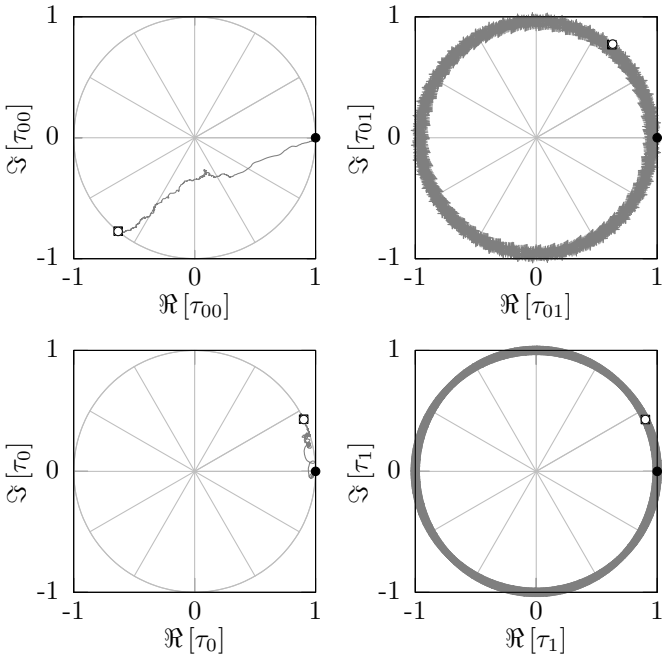

FIG. 9: Phase dynamics induced by the optimized pulse ($T = 800\,\text{ps}$) in the complex plane for the two-qubit single-qubit states, analogously to Fig. 6.

for $T = 50\,\text{ps}$ shows somewhat more features within the peak which is attributed to the better spectral resolution for larger T. For $T = 800\,\text{ps}$, the spectrum of the optimal pulse consists of a narrow peak at the $|0\rangle \to |a\rangle$ transition frequency and sidebands. These sidebands remain sufficiently close to the $|0\rangle \to |a\rangle$ transition, that resonant excitation into other electronic states can be excluded, cf. Fig. 3. The phase dynamics induced by the optimized pulse of Fig. 8 are shown in Fig. 9. Since the target phases include the natural time evolution, their locations in Fig. 9 differ from those in Fig. 6. The overlap of the final states (black square) and the target states (open circle) confirms success of the optimization. All phases end up on the unit circle demonstrating that no leakage from the quantum register occurs at the end of the gate for $T = 800\,\text{ps}$.

We also carried out optimizations for non-local target phases that are a fraction of π such as $\frac{\pi}{2}$ or $\frac{\pi}{3}$. If high-fidelity implementations of such fractional phasegates are found, several of these gates can be combined sequentially to yield a total non-local phase of π. However, for short gate operation times, optimization for non-local target phases smaller than π did not prove any more successful than optimization for π. In particular, population of excited trap states at the end of the gate could not be avoided for fractional phasegates either. Moreover, we investigated whether pulses driving multi-photon transitions, for example pulses with their central frequency a third of $|0\rangle \to |1\rangle$ transition frequency, yield better fidelities for short gate operation times. However, we did not observe any substantial difference in the results compared to the pulses reported in Figs. 5, 7, and 8. These additional investigations confirm that for our example of two ultracold calcium atoms in an optical lattice, the limits on the gate operation time is set by the requirement to restore the ground vibrational state of the trap.

B. Optimization for Two Atoms at Long Distance under Strong Dipole-Dipole Interaction

To determine whether it is really the ground state motion in the trap and not the non-local interaction in the excited state that sets the speed limit for two atoms resonantly excited to an interacting state, we vary the interaction strength C_3 of the dipole-dipole interaction potential,

$$\hat{\mathbf{V}}(R)_{0a} = \hat{\mathbf{V}}(R)_{a0} = -\frac{C_3}{R^3}\,, \tag{18}$$

keeping the trap frequency constant. We consider the atoms to be separated by $d = 200\,\text{nm}$ which corresponds to a realistic optical lattice in the UV regime. In order to keep the overlap of the ground state wave functions smaller than 10^{-4} at a distance of 200 nm the trap fre-

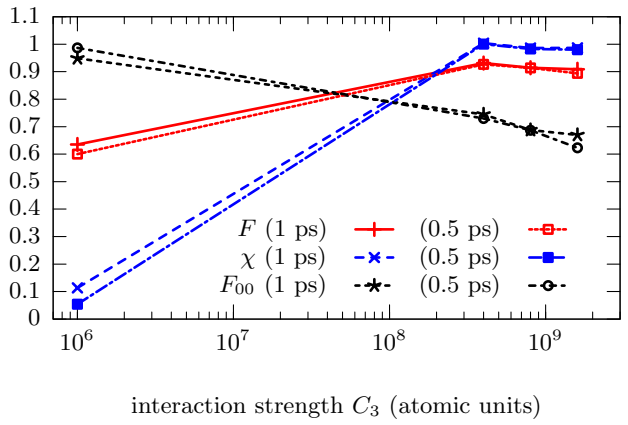

FIG. 10: (color online) Fidelity F, non-local phase χ and vibrational fidelity, i.e. projection onto the vibrational target state, F_{00} for increasing interaction strength C_3 in the excited state for two different gate times T. All optimizations have converged to $\Delta F < 1 \times 10^{-4}$ The interatomic distance is $d = 200\,\mathrm{nm}$.

quency has to be set to at least 250 kHz. This corresponds to $T_v \approx 2\,\mathrm{ns}$.

For the interaction potential of two calcium atoms in the $B^1\Sigma_u^+$ state used in Sec. III A, the C_3 coefficient takes a value of $16.04\,\mathrm{a.u.} = 0.5217 \times 10^3\,\mathrm{nm^3 cm^{-1}}$ [23, 24, 31]. This results in an interaction energy of about $4\,\mathrm{cm^{-1}}$ at $d = 5\,\mathrm{nm}$. Based on the results of Sec. III A, we know that such an interaction energy is sufficient to yield a non-local phase in a few tens of picoseconds. For $d = 200\,\mathrm{nm}$, the same interaction energy is obtained by choosing C_3 to be roughly $1 \times 10^6\,\mathrm{a.u.}$ Just for comparison, the C_3 coefficient for highly excited Rydberg states is about $3 \times 10^6\,\mathrm{a.u.}$, resulting in an interaction energy of about $1.3 \times 10^{-3}\,\mathrm{cm^{-1}}$ at a typical distance of $4\,\mu\mathrm{m}$ for two atoms trapped in optical tweezers [32].

We vary the C_3 coefficient from $1 \times 10^6\,\mathrm{a.u.}$ to $1 \times 10^9\,\mathrm{a.u.}$ If the gate duration is solely determined by the requirement of a sufficiently strong interaction to realize the non-local phase, we expect to find high-fidelity implementations with optimal control by increasing the C_3 coefficient. In particular, we pose the question whether picosecond and sub-picosecond gate durations can be achieved given that the interaction is sufficiently strong, i.e. given that the C_3 coefficient is sufficiently large. Based on the results of Sec. III A where a non-local phase of π was achieved within 50 ps, we estimate that C_3 needs to be increased from 1×10^6 by a factor of 50 (100) to obtain a high-fidelity gate for a duration of 1 ps (0.5 ps).

Figure 10 presents optimization results for a controlled phasegate with gate operation times of $T = 0.5\,\mathrm{ps}$ and $T = 1\,\mathrm{ps}$. The central frequency of the guess pulse was adjusted in each case to compensate for the increased interaction energy and ensure resonant excitation. The grid parameters were chosen to be $R_{\min} = 5\,\mathrm{a_0}$, $R_{\max} = 13000\,\mathrm{a_0} \approx 688\,\mathrm{nm}$, and $N_R = 2048$. This choice of $R_{\max}$ guarantees that at least fifty eigenstates of the trap are accurately represented. We verified that the grid is sufficiently large, i.e., the wave packet does not reach the boundaries of the grid during propagation. Moreover we checked that doubling the number of grid points did not yield substantially different results. Figure 10 clearly shows that increasing the interaction strength leads to larger non-local phases. A non-local phase of π is reached for $C_3 = 4 \times 10^8\,\mathrm{a.u.}$ However, increasing the interaction strength also results in a complete loss of control over the motional degree of freedom, with the vibrational fidelity F_{00} reduced to 75% and below. A stronger interaction in the excited state accelerates the wave packet more, increasing its vibrational excitation. This results in a larger spread over many trap states upon the wave packet's return to the ground state. Since 0.5 ps or 1 ps are much, much shorter than the time scale of the motion in the trap, T_v, the optimization algorithm cannot resolve the eigenstates of the trap. Thus it cannot identify the target F_{00} which is consequently missed completely. Note that trap frequencies up to a few MHz are possible and imply shorter T_v. Nevertheless, any realistic trap frequency results in vibrational time scales much larger than a few picoseconds. While excited state potentials providing for a strong interaction between two neutral atoms exist, resonant excitation into such an excited state will not yield an ultrafast non-local gate due to coupling with the motional degree of freedom, unless we consider a gate scheme that is completely insensitive to vibrational excitations

IV. SUMMARY AND CONCLUSIONS

We have studied high-fidelity implementations of a controlled phasegate for two trapped ultracold atoms via resonant optical transitions to an electronically excited state with long-range diatomic interaction. To the best of our knowledge, we have for the first time explicitly accounted for the detailed R-dependence of the interaction and thus for the coupling between electronic and nuclear dynamics that may cause leakage out of the quantum register. We have employed optimal control theory to calculate laser pulses that carry out the gate. This has allowed us to determine gate implementations of basically arbitrarily high fidelity provided the gate operation time is sufficiently long (and at the same time short enough to neglect dissipation). Our main goal was to achieve the fastest possible gate implementation and to identify what limits the gate operation time, i.e., to determine the quantum speed limit for a controlled phasegate for two neutral trapped atoms.

The standard reasoning considers the interaction strength to be the limiting factor, i.e., the gate operation time is estimated by the inverse of the two-qubit interaction. Our calculations show that a second time scale might come into play: For resonant excitation, the interaction between the two atoms causes a coupling be-

tween electronic and nuclear dynamics. This induces vibrational excitation which can be carried away by the laser pulse only if the target state is fully resolved during the optimization. The gate operation time is thus limited either by the two-qubit interaction strength or by the vibrational motion in the trap, which ever one of the two yields the larger time.

This finding has important implications for the design of two-qubit gates where the qubits are carried by neutral atoms. For example, excitation of atoms into Rydberg states yields an interaction that one might expect to allow for nanosecond to sub-nanosecond gate operation times. However, the motional state of the atoms needs to be restored at the end of the gate, and traps with sub-nanosecond vibrational motion seem difficult to realize. Thus the question of how an ultrafast two-qubit gate can be realized in a scalable setup still remains open.

Acknowledgments

We would like to thank Peter Zoller for many stimulating discussions. Financial support from the Deutsche Forschungsgemeinschaft (Grant No. KO 2302), as well as the BMBF (project QUOREP) and the EC (IP AQUTE) is gratefully acknowledged .

Appendix A: Reduced Optimization Scheme

Since the dynamics relevant for obtaining a non-local phase involves only the $|00\rangle$ state out of the four two-qubit states, cf. Fig. 2, we can reduce our full model, Eq. (2), to one describing only the left-most column of Fig. 2. This is a direct consequence of optimizing for a diagonal two-qubit gate. We are then operating in a $4N_R$-dimensional Hilbert space instead of a $3 \times 3 \times N_R$-dimensional Hilbert space. However, care must be taken to extract the correct non-local phase χ. The phase ϕ_{00} describing the time evolution of the two-qubit $|00\rangle$ state alone is not sufficient to obtain the non-local phase χ since ϕ_{00} contains contributions from both the single-qubit and two-qubit dynamics. We therefore need to augment our reduced model for the dynamics starting from the $|00(R)\rangle$ by a two-level system ($|0\rangle$, $|a\rangle$). This captures the purely single-qubit dynamics in the phase ϕ_0. The non-local phase is then obtained as the difference between ϕ_{00} and (twice) ϕ_0, see Table I. The optimization targets for the full model and the reduced model are also listed in Table I. They correspond to the unitary transformation for the full model and to two state-to-state transitions for the reduced model. Note that this type of state-to-state transition requires a phase-sensitive functional such as the one in Eq. (7). We have checked numerically that the full and reduced model are indeed equivalent: Propagating the Schrödinger equation with an optimal pulse obtained for the reduced model but employing the full Hamiltonian, Eq. (2), we obtained the same fidelity as for the reduced model.

	full	reduced
target	$\|00\rangle \to e^{i(\phi+\phi_T)}\|00\rangle$ $\|01\rangle \to e^{i\phi_T}\|01\rangle$ $\|10\rangle \to e^{i\phi_T}\|10\rangle$ $\|11\rangle \to e^{i\phi_T}\|11\rangle$	$\|00\rangle \to e^{i(\phi+\phi_T)}\|00\rangle$ $\|0\rangle \to e^{i\phi_T/2}\|0\rangle$
gate phases	ϕ_{00} $\phi_{10} = \phi_{01}$ ϕ_{11}	$= \phi_{00}$ $= \phi_0 + \phi_1$ $= 2\phi_1$
non-local phase	$\chi = \phi_{00} - \phi_{01} - \phi_{10} + \phi_{11}$	$\chi = \phi_{00} - 2\phi_0$

TABLE I: Comparison between the full model and the reduced model for optimization of a controlled phasegate.

[1] M. Nielsen and I. L. Chuang, *Quantum Computation and Quantum Information* (Cambridge University Press, 2000).

[2] D. Jaksch, H.-J. Briegel, J. I. Cirac, C. W. Gardiner, and P. Zoller, Phys. Rev. Lett. **82**, 1975 (1999).

[3] T. Calarco, E. A. Hinds, D. Jaksch, J. Schmiedmayer, J. I. Cirac, and P. Zoller, Phys. Rev. A **61**, 022304 (2000).

[4] M. Anderlini, P. J. Lee, B. L. Brown, J. Sebby-Strabley, W. D. Phillips, and J. V. Porto, Nature **448**, 452 (2007).

[5] S. Trotzky, P. Cheinet, S. S. Fölling, M. Feld, U. Schnorrberger, A. M. Rey, A. Polkovnikov, E. A. Demler, M. D. Lukin, and I. Bloch, Science (2008).

[6] D. Jaksch, J. I. Cirac, P. Zoller, S. L. Rolston, R. Côté, and M. D. Lukin, Phys. Rev. Lett. **85**, 2208 (2000).

[7] L. Isenhower, E. Urban, X. L. Zhang, A. T. Gill, T. Henage, T. A. Johnson, T. G. Walker, and M. Saffman, Phys. Rev. Lett. **104**, 010503 (2010).

[8] T. Wilk, A. Gaëtan, C. Evellin, J. Wolters, Y. Miroshnychenko, P. Grangier, and A. Browaeys, Phys. Rev. Lett. **104**, 010502 (2010).

[9] C. P. Koch, E. Luc-Koenig, and F. Masnou-Seeuws, Phys. Rev. A **73**, 033408 (2006).

[10] C. P. Koch and R. Moszyński, Phys. Rev. A **78**, 043417 (2008).

[11] J. P. Palao and R. Kosloff, Phys. Rev. A **89**, 188301 (2002).

[12] J. P. Palao and R. Kosloff, Phys. Rev. A **68**, 062308 (2003).

[13] D. Tannor, V. Kazakov, and V. Orlov, in *Time-dependent quantum molecular dynamics*, edited by J. Broeckhove and L. Lathouwers (Plenum, 1992), pp. 347–360.
[14] J. Somlói, V. A. Kazakov, and D. J. Tannor, Chem. Phys. **172**, 85 (1993).
[15] W. Zhu, J. Botina, and H. Rabitz, J. Chem. Phys. **108**, 1953 (1998).
[16] C. M. Tesch and R. de Vivie-Riedle, Phys. Rev. Lett. **89**, 157901 (2002).
[17] R. S. Judson and H. Rabitz, Phys. Rev. Lett. **68**, 1500 (1992).
[18] W. C. Campbell, J. Mizrahi, Q. Quraishi, C. Senko, D. Hayes, D. Hucul, D. N. Matsukevich, P. Maunz, and C. Monroe, Phys. Rev. Lett. **105**, 090502 (2010).
[19] S. Lloyd, Nature **406**, 1047 (2000).
[20] L. B. Levitin and T. Toffoli, Phys. Rev. Lett. **103**, 160502 (2009).
[21] T. Caneva, M. Murphy, T. Calarco, R. Fazio, S. Montangero, V. Giovannetti, and G. E. Santoro, Phys. Rev. Lett. **103**, 240501 (2009).
[22] M. M. Boyd, A. D. Ludlow, S. Blatt, S. M. Foreman, T. Ido, T. Zelevinsky, and J. Ye, Phys. Rev. Lett. **98**, 083002 (2007).
[23] B. Bussery-Honvault, J.-M. Launay, and R. Moszynski, Phys. Rev. A **68**, 032718 (2003).
[24] B. Bussery-Honvault and R. Moszynski, Mol. Phys. **104**, 2387 (2006).
[25] V. Kokoouline, O. Dulieu, R. Kosloff, and F. Masnou-Seeuws, J. Chem. Phys. **110**, 9865 (1999).
[26] K. Willner, O. Dulieu, and F. Masnou-Seeuws, J. Chem. Phys. **120**, 548 (2004).
[27] S. Kallush and R. Kosloff, Chem. Phys. Lett. **433**, 221 (2006).
[28] R. Kosloff, Annu. Rev. Phys. Chem. **45**, 145 (1994).
[29] J. Zhang, J. Vala, S. Sastry, and K. B. Whaley, Phys. Rev. A **67**, 042313 (2003).
[30] B. Kraus and J. I. Cirac, Phys. Rev. A **63**, 062309 (2001).
[31] C. Degenhardt, T. Binnewies, G. Wilpers, U. Sterr, F. Riehle, C. Lisdat, and E. Tiemann, Phys. Rev. A **67**, 043408 (2003).
[32] A. Gaëtan, Y. Miroshnychenko, T. Wilk, A. Chotia, M. Viteau, D. Comparat, P. Pillet, A. Browaeys, and P. Grangier, Nature Physics **5**, 115 (2009).